JOURNAL OF COMPUTATIONAL PHYSICS 82, 289–297 (1989)

# A Three-Dimensional Computational Method for Blood Flow in the Heart. II. Contractile Fibers

DAVID M. MCQUEEN AND CHARLES S. PESKIN

*Courant Institute of Mathematical Sciences, New York University, 251 Mercer Street, New York, New York 10012*

Received March 2, 1988; revised July 15, 1988

This paper is the second in a series that describes the development of a 3-dimensional computer model of the heart. The problem studied here is that of a *contractile* fiber-wound toroidal tube immersed in a viscous incompressible fluid. A wave of contraction propagates around the tube, and this results in peristaltic pumping of the internal fluid in the direction of the wave. When the contraction is sufficiently strong, there is a small region of entrained fluid that is convected along at the speed of the wave. 

## INTRODUCTION

This paper is the second in a series that describes a computational method for the coupled equations of motion of a viscous incompressible fluid containing an immersed system of elastic or contractile fibers. Part I [1] introduces the method and applies it to the damped vibrations of a fiber-wound toroidal tube with time-independent elastic properties. The present paper considers the case of time-dependent elasticity, in which the fibers are contractile. The method is applied to a fiber-wound tube in which waves of contraction of the fibers are used to pump fluid around the tube (peristaltic pumping). Such contractile fibers are a critical ingredient in the computer model of the heart which will be the subject of Part III.

## METHODS

The computational method has been fully described in [1], except for those aspects that are related to time-dependent elastic properties, but a brief summary will be given here to help orient the reader. The computational method used here and in [1] solves the coupled equations of a viscous, incompressible fluid and an immersed system of elastic or contractile fibers. The fluid equations are solved on a fixed cubic lattice, and the fibers are modeled by 1-dimensional arrays of moving points. The fiber points are not required to coincide with the lattice points that are used for the fluid computation. Interaction between the fibers and the fluid is handled as follows: First the fiber points move at the local fluid velocity, which is



0021-9991/89 $3.00

obtained by interpolation from the lattice points of the fluid computation. Second, the forces generated in the fibers are applied to the surrounding fluid. In both cases, the weights that define the coupling between fiber points and fluid points are derived from a computational model of the Dirac $\delta$-function.

The forces that are applied by the fibers to the fluid are computed from the fiber elasticity (which was time-independent in [1] but time-dependent here). Adjacent points along a fiber are thought of as being connected by springs, so that the force on each fiber point is the result of the forces generated in the two springs connected to that point. The fiber points being massless (see [1]), this force is transmitted to the fluid.

In [1], the fiber forces were derived from an elastic energy function of the form

$$E(\dots \mathbf{X}_k \dots) = \sum_k e\left(\frac{|\mathbf{X}_{k+1} - \mathbf{X}_k|}{\Delta s}\right) \Delta s, \tag{1}$$

where

$$e(q) = \int_0^q \sigma(q')\, dq'. \tag{2}$$

In these equations, $\mathbf{X}_k$ is the position of the $k$th fiber point, $\Delta s$ is the unstressed resting length of the springs that connect adjacent fiber points, $e$ is the elastic energy of the fiber per unit unstressed length, $\sigma$ is the fiber tension, and $q$ is a dummy variable corresponding to $|\mathbf{X}_{k+1} - \mathbf{X}_k|/\Delta s$ so that $q - 1$ is the fiber strain.

Here, we introduce explicit time dependence (and also explicit dependence on the Lagrangian position). This leads to an energy function of the form

$$E(\dots \mathbf{X}_k \dots, t) = \sum_k e_k\left(\frac{|\mathbf{X}_{k+1} - \mathbf{X}_k|}{\Delta s}, t\right), \tag{3}$$

where

$$e_k(q, t) = \int_0^q \sigma_k(q', t)\, dq'. \tag{4}$$

The particular functions $\sigma_k$ that we use have the form

$$\sigma_k(q, t) = \begin{cases} S_k(t)(q\,\Delta s - R_k(t)), & r \geqslant R_k(t) \\ 0, & r \leqslant R_k(t), \end{cases} \tag{5}$$

where $S_k(t)$ is the stiffness and $R_k(t)$ is the resting length of the spring that joins point $k$ and point $k+1$. The functions $S_k(t)$ and $R_k(t)$ are given in advance. At any particular time step they have constant known values, so the computational method is not changed by the fact that these values are different at different time steps.

## RESULTS

We consider the fiber-wound toroidal tube of Ref. [1], but here we let a wave of contraction propagate along this tube driving fluid around it. Although such a wave of contraction could be generated by varying either the stiffness or the resting-length parameters, we choose to hold the stiffnesses constant and to vary the resting lengths as described below.

In the following, let $R_k^0$ be the *relaxed* resting length of link $k$, and let $\theta_k^0$ be the Lagrangian position of this link expressed in terms of angle about the symmetry axis in the equilibrium configuration of the tube. Then we impose the time variation on the resting length of link $k$,

$$R_k(t) = R_k^0(1 - \alpha(t - \theta_k/c)\,\beta(t)), \tag{6}$$

where $\alpha(t)$ is a periodic step function with period $T = T_S + T_D$ that satisfies

$$\alpha(t) = \begin{cases} \alpha^*, & 0 < t < T_S \\ 0, & T_S < t < T = T_S + T_D \end{cases} \tag{7}$$

$$\alpha(t + T) = \alpha(t) \tag{8}$$

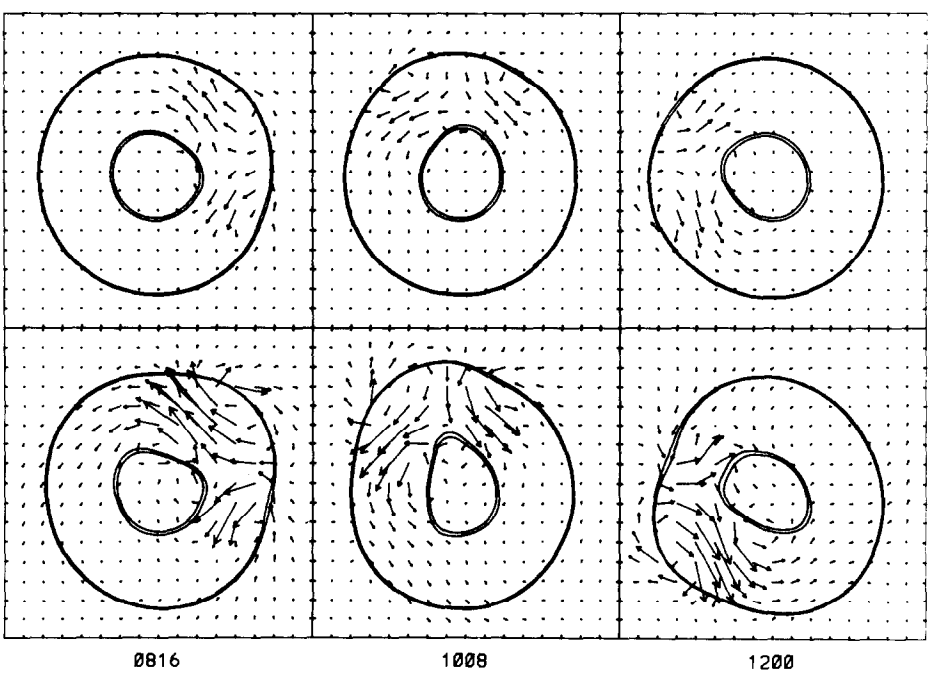


FIG. 1. Cross section of torus and velocity vectors in the laboratory frame. Top row: weak contraction ($\alpha^* = 0.25$), bottom row: strong contraction ($\alpha^* = 0.625$). Three selected time steps are shown in each case. The wave of contraction rotates counterclockwise.

and where

$$\beta(t) = (1 - e^{-t/\tau}). \tag{9}$$

(The factor $\beta(t)$ is included merely to provide a smooth start-up. For $t \gg \tau$, $\beta(t) \approx 1$.) The parameter $c$ gives the wave speed in radians per unit time. Since there must be an integer number of wavelengths in $2\pi$ radians, we require that

$$cT = 2\pi/n. \tag{10}$$

In practice we take $n = 1$, so that is only one band of contraction moving around the torus. The parameter $\alpha^*$ sets the overall strength of the contraction. Once the wave is up to full strength ($\beta \approx 1$), then the fibers in the active region have rest lengths which have been reduced by a fraction $\alpha^*$ from their passive rest length. Note that $\alpha^*$ must satisfy $0 \leqslant \alpha^* \leqslant 1$. At $\alpha^* = 0$ there is no contraction at all, while at $\alpha^* = 1$ the rest length shrinks to zero during the active phase of the contraction.

The effect of Eq. (6) is to send a wave of contraction propagating around the torus. At any point on the torus, $T_S$ is the duration of the active phase ("systole", and $T_D$ is the duration of the passive phase ("diastole"). The temporal period of the wave is $T = T_S + T_D$ and the wavespeed (in radians per unit time) is $c$.

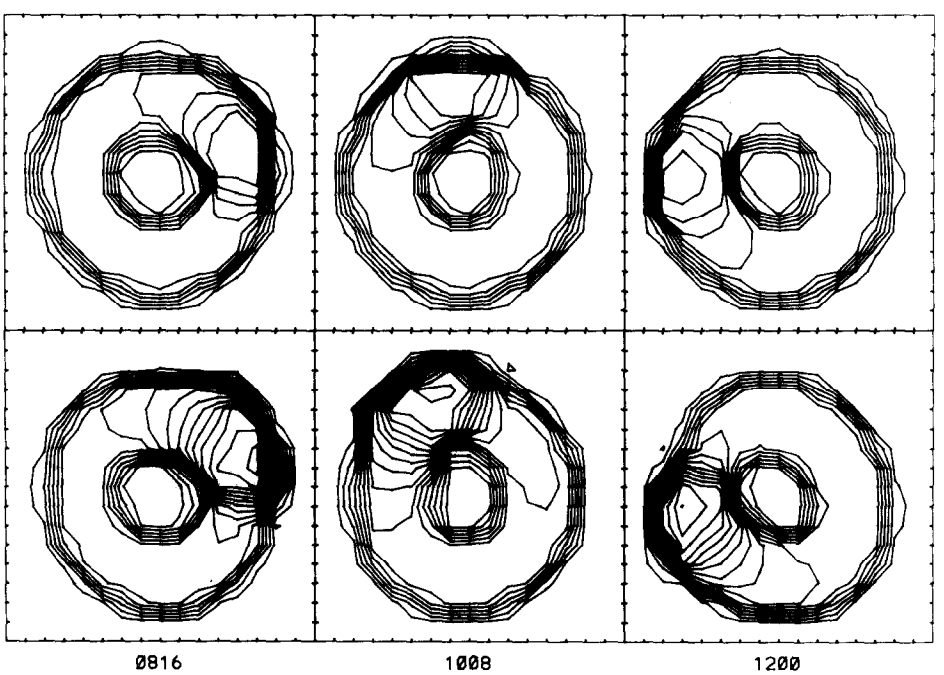


FIG. 2. Pressure contours corresponding to the velocity vectors shown in Fig. 1.

Let us now consider the computed solution to the problem outlined above. Figure 1 shows computed velocity vectors in the plane $z = 0$. The cross section of the torus in this plane is also shown. Two different strengths of contraction are depicted in the figure: the top row has $\alpha^* = 0.25$ while the bottom row has $\alpha^* = 0.625$. Each of the three columns corresponds to a selected time step. In the time interval covered by the figure, the wave makes roughly half a turn around the torus. Note the larger velocity vectors and the greater deformation of the torus in the bottom row, where the contraction is stronger. Notice, too, the asymmetry of the velocity vectors. In general the vectors in the direction of wave propagation (counterclockwise in the figure) are larger than those in the reverse direction.

Figure 2 shows computed pressure contours in the plane $z = 0$. The times and contraction strengths are the same as in Fig. 1. Here we do not explicitly draw in the cross section of the tube, since the pressure contours mark it very well. Note the pressure maximum in the interior of the tube that moves around with the wave of contraction. As with the velocity vectors there is an asymmetry here: the pressure gradient is steeper in the backward direction than in the forward direction from the

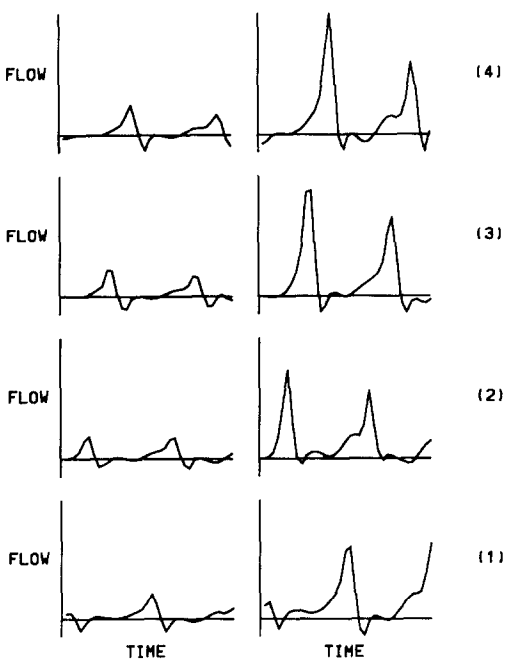


FIG. 3. Flow (volume/time) through the torus lumen as a function of time at four separate stations located 90° apart. Left column shows results for weak contraction; right column for stronger contraction. Reading up through the stations from (1) through (4), one can follow the progress of the wave, which makes two complete cycles in the course of the computational experiment. Note net forward flow (especially for the stronger contraction); this indicates effectiveness of the contractile tube as a peristaltic pump.

pressure maximum. (This is the opposite of what one might guess from the lengths of the velocity vectors.)

Figure 3 shows the flux through the tube (volume/time) at four stations located 90° apart. The left-hand column shows the weaker contraction while the right-hand column shows the stronger contraction. Reading up either column one can follow the progress of the wave, which goes twice around the tube over the duration of the computer experiment. At each station, the imminent arrival of the wave is indicated by a strong positive peak consisting of fluid that is propelled forward ahead of the constricted region. This is followed by a smaller negative peak of fluid that flows backward through the constriction itself. The net flow is positive (this is particularly clear for the stronger contraction), which indicates that the wave of contraction succeeds in pumping fluid around the tube.

Overall, Figs. 1–3 do not show qualitative differences between the two contraction strengths. Such differences are revealed, however, if we switch to a frame of reference rotating with the wave. In such a frame, the flow is nearly steady and the constriction appears to stand still, although the tube walls slide tangent to them-

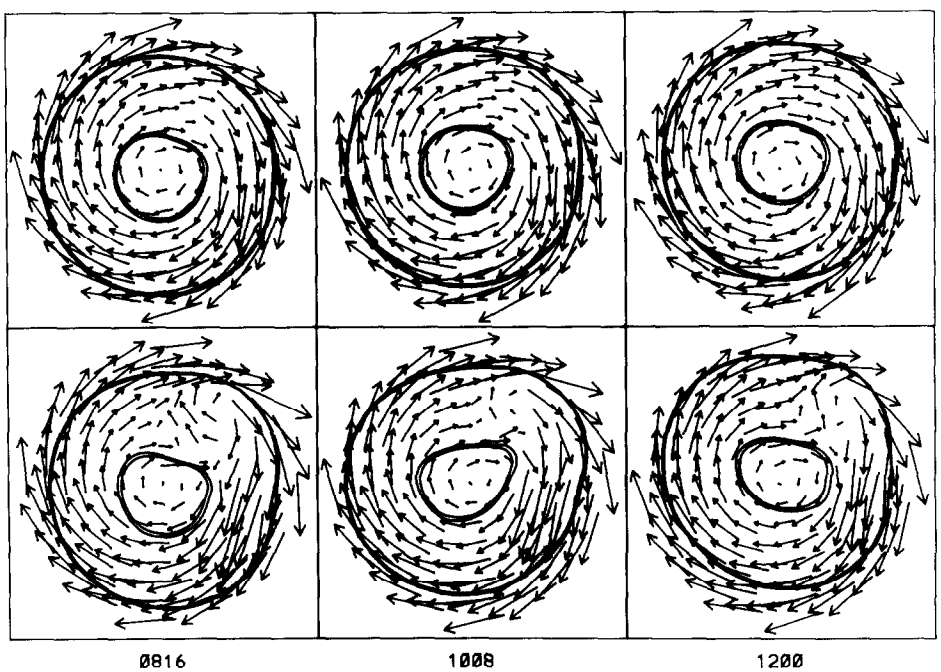


FIG. 4. Velocity vectors in a frame of reference rotating with the wave (same format as Fig. 1). In the top row (weaker contraction), the flow is essentially a rigid-body rotation; there is little visual evidence of the active contractile region. In the bottom row (stronger contraction) there is a small zone of recirculation just ahead of the constriction. Note similarity of the flow pattern at different time steps. This indicates approximately steady flow in the wave frame.

selves in the clockwise direction (as viewed in our figures). We call this frame of reference the "wave frame."

Figure 4 shows velocity vectors in the wave frame. The top row (weaker contraction) looks almost like a rigid rotation; it is hard to see the effects of the constriction, which manifests itself only as a reduced velocity of flow within the tube at about 1–2 o'clock. In the bottom row, however, there appears to be a small zone of recirculation at the same location. This zone of recirculation is even more evident in Fig. 5, which shows streaklines (particle trajectories) in the wave frame. Since the flow is nearly steady in the wave frame (compare the three times steps shown) streaklines are essentially the same as streamlines (curves that are everywhere parallel to the velocity field at some instant).

Figures 4–5 suggest that, in the case of the stronger contraction, particles may become trapped in the recirculation zone and be convected around the tube at the speed of the wave. This is a remarkable phenomenon, since the wall motion that generates the wave certainly does not involve any large-scale transport of the material points of the wall, which move primarily in and out and which suffer only slight longitudinal displacement.

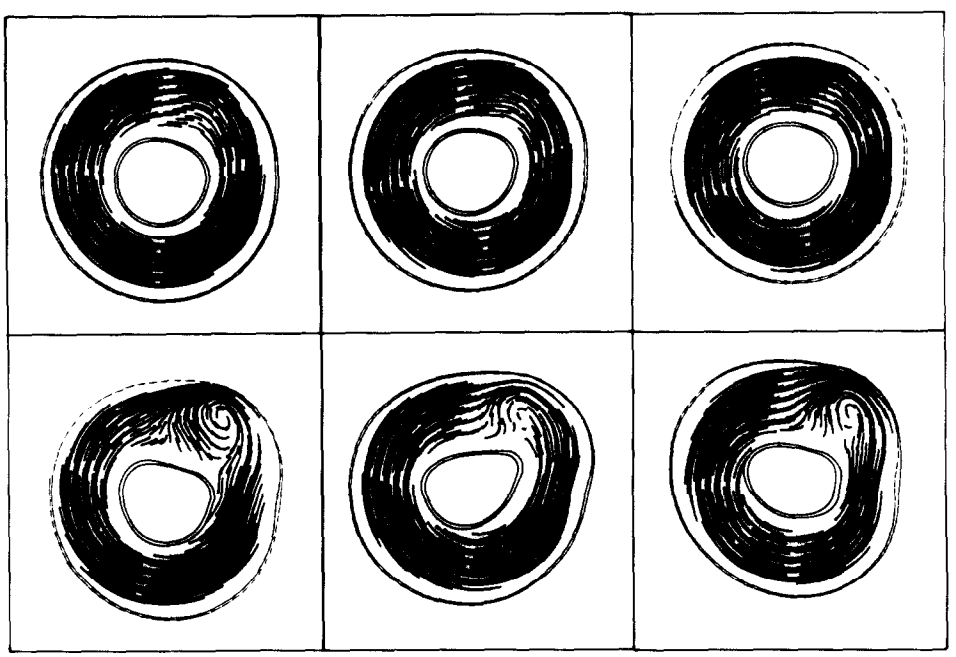


FIG. 5. Streaklines (particle trajectories) in a frame of reference rotating with the wave. (Since the flow is approximately steady in the wave frame, *streak*lines are essentially the same as *stream*lines.) As in Fig. 4, note the zone of recirculation just ahead of the wave in the case of the stronger contraction. Fluid in this zone has been entrained by the wave. In the laboratory frame, such fluid is convected around the tube at the speed of the wave.

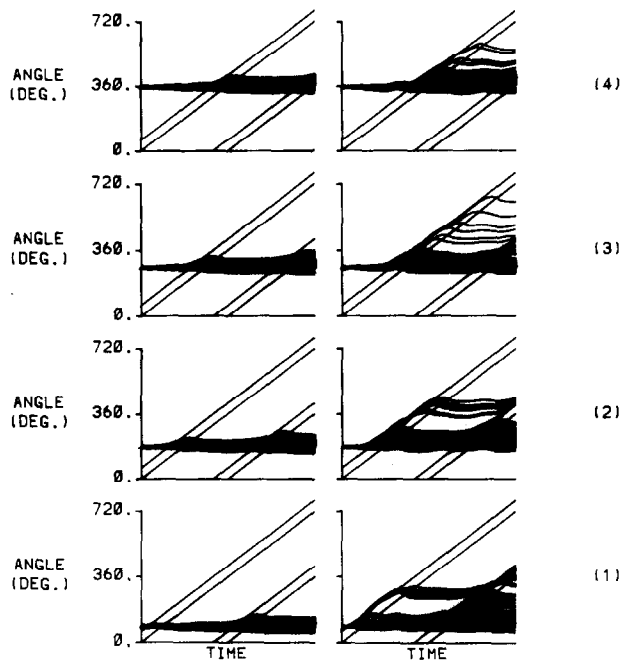


FIG. 6. Particle trajectories (angular position vs time). Left column: weak contraction. Right column: strong contraction. Each row shows particles which are initially distributed over the torus lumen in a cross section corresponding to one of the four stations of Fig. 3. (These stations are located at intervals of 90° around the tube.) Straight diagonal lines indicate the trajectory of the front and back of the wave. (Each frame shows two periods in space and two periods in time.) In the left column, note that particles are only slightly displaced forward as the wave goes by: In the right column, by contrast, many particles are caught by the front of the wave and carried for substantial distances around the tube before being left behind. (There is one particle at station 3 which makes a full 360° circumnavigation of the tube.) These trapped particles move at essentially the speed of the wave, so they must be caught in the recirculation zone that is evident in Fig. 5. The fact that particles enter and leave that zone, however, is evidence of a 3-dimensional flow pattern in which the recirculation zone is connected by streamlines with the rest of the fluid (even in the wave frame).

Such particle convection at the speed of the wave (in the case of the stronger contraction) is confirmed in Fig. 6 which plots the angular trajectories of fluid particles and of the wave itself. The format of Fig. 6 is similar to that of Fig. 3, in which flows, were plotted at four separate stations for each of the two contraction strengths. Here each frame plots the angular history of particles that start out distributed over the cross section of the tube at one of these four stations. The straight diagonal lines indicate the angular trajectories of the front and back of the wave.

In the case of the weaker contraction (left column), particles are pushed forward slightly by the passage of the wave, but no particles are entrapped for any significant time. The dispersion in particle displacements is presumably caused by the variable initial location of the particles over the cross section of the torus. In the

case of the stronger contraction (right column), many particles are caught by the front of the wave and carried along at the speed of the wave for variable but substantial distances before they are left behind. (One particle which starts at station 3 manages to get all of the way around the tube before dropping behind.) Presumably, the results depicted in the right-hand column of Fig. 6 reflect a complex 3-dimensional flow pattern in which particles get caught up in the recirculation zone for a while and then leave it via the third dimension.

In summary, for sufficiently strong contractions we find a small recirculation zone just ahead of the wave in which trapped fluid is propelled around the torus at the speed of the wave. Such a zone is in fact predicted by the simplified theory of Ref. [2], which is based on Poiseuille flow. In that theory, however, the recirculation zone is not localized at the front of the wave but fills the entire relaxed portion of the tube. Moreover, there is no mechanism in the Poiseuille flow theory to account for particles entering and leaving the recirculation region. Thus our results confirm a key qualitative prediction of [2]: the fact that some fluid will be convected at the speed of the wave when the contraction is sufficiently strong. At the same time, these results also produce important modifications of the picture that emerges in [2], since we find only a small recirculation zone poised at the front of the wave and since we find that the trapping of fluid particles in the recirculation zone is only temporary.

## Conclusions

In Ref. [1], we presented a computational method that solves the 3-dimensional Navier–Stokes equations in the presence of an immersed system of elastic fibers. The principal conclusion of the present paper is that this method is also applicable to the case in which the fibers have time-dependent elastic parameters and hence are capable of active mechanical behavior. This is a crucial step in the construction of a 3-dimensional computer model of the heart.

## Acknowledgments

This work was supported by the N.I.H. under research grant HL17859 and also by the N.S.F. under research grant DMS8312229. Computation was performed on the Cray 2 at the Minnesota Supercomputer Center. We are indebted to the staff of the Center for their ongoing technical support of this project and especially for the preparation of a computer-generated videotape that illustrates in motion and in various perspective views the 3-dimensional results of this study.

## References

1. C. S. Peskin and D. M. McQueen, *J. Comput. Phys.* **81**, 372 (1989).
2. S. Childress, "Aspects of Physiological Fluid Mechanics. II. Peristaltic Pumping," *Mathematical Aspects of Physiology*, Lectures in Applied Mathematics, Vol. 19, edited by F. Hoppensteadt (Amer. Math. Soc., Providence, RI, 1981), p. 151.